Journal of Materials Chemistry A

PAPER

View Article Online
View Journal | View Issue

Cite this: J. Mater. Chem. A, 2018, 6, 20383

Thermal stability of Sn anode material with non-aqueous electrolytes in sodium-ion batteries†

Yongho Lee,[ad] Hyojun Lim,[ab] Sang-Ok Kim,[a] Hyung-Seok Kim,[a] Ki Jae Kim,[c] Kwan-Young Lee[d] and Wonchang Choi *[ab]

The thermal behavior of fully lithiated and sodiated Sn electrodes cycled in a $MePF_6$ (Me = Li or Na)-based electrolyte was studied using differential scanning calorimetry (DSC). The sodiated Sn electrode cycled in the $NaPF_6$-based electrolyte showed a thermal reaction with much greater heat generation (1719.4 J g^{-1}) during the first exothermic reaction corresponding to the thermal decomposition reaction of the solid electrolyte interface (SEI) layer, compared to that of the lithiated Sn electrode (647.7 J g^{-1}) in the $LiPF_6$-based electrolyte because of the formation of a thicker surface film on the Sn electrode. The $NaPF_6$-based electrolyte yielded a slightly less conductive and/or a thicker SEI layer than the $NaClO_4$-based electrolyte, resulting in the intense thermal decomposition of the SEI layer. The DSC results for the fully sodiated Sn electrode cycled in FEC-containing electrolytes clearly demonstrate that an exothermic reaction corresponding to the SEI decomposition mostly disappears because of the formation of a thermally stable and thin SEI layer on active materials *via* the electrochemical decomposition of FEC. X-ray photoelectron spectroscopy reveals the formation of SEI with a relatively high proportion of NaF, which is known to be a thermally stable inorganic solid at high temperatures.

Received 13th August 2018
Accepted 21st September 2018

DOI: 10.1039/c8ta07854h

rsc.li/materials-a

Introduction

Lithium ion batteries (LIBs), which dominate the portable electronic market, are prime candidates to power the next generation of electric vehicles.[1–11] LIBs offer the highest energy density and output voltage of all rechargeable battery technologies.[1–6] Although LIBs have several advantages, lithium deposits are mainly distributed in South America, and the limited lithium reserves are insufficient to meet the ever-increasing demand for various applications. Thus, sodium-ion batteries (SIBs) are considered to be an alternative to LIBs, as sodium is the fourth most abundant element in the Earth's crust, is non-toxic, and is cheaper than lithium.[1–5,7,12,13]

However, some LIB host candidates cannot accommodate sodium ions; for example, graphite, which is considered as a promising LIB anode material, is difficult to utilize in SIB systems, owing to the larger ionic radius of sodium.[3,4,14–19] Therefore, SIB anode materials have been mainly limited to nongraphitic hard carbon, where sodium ions absorb/desorb at the surface of the nanoscopic pores of hard carbon.[20–31] However, these materials have relatively low specific capacities (<300 mA h g^{-1}).

As with Li storage, a material based on a Na-alloying reaction can also store Na ions.[4,6,14,19,31–34] Metallic Sn has attracted significant attention as a SIB anode material because of its high Na-storage capacity of 847 mA h g^{-1}.[4,6,14,31,33] However, alloyed anodes usually undergo a large volume change during Na^+ extraction, which leads to cracks and pulverization of the particles, and a loss of electric contact between the active materials and the current collector.[31–34] Considerable efforts have been made to solve these issues.[31–34]

Although Sn-based materials have been studied and developed as promising anode materials because of their high capacity, their thermal stability is questionable. The safety issues of SIB anode materials pose major technological challenges, particularly for large-scale applications. Considering the high activity of sodium metal, the risk of thermal reactions related to charged anodes is thought to be higher in SIBs than in LIBs.[35] Moreover, it has been suspected that the stable solid electrolyte interface (SEI) does not form readily on the anode surface in Na-ion batteries. This also increases the thermal risk for the cells because the chemical structure and morphology of the SEI layer can critically influence the safety of the batteries.[25–27,30,35–39] Therefore, the investigation of the thermal properties for sodiated Sn electrodes is important for the development and practical application of SIBs.

[a]Center for Energy Storage, Korea Institute of Science and Technology, 5, Hwarang-ro 14-gil, Seongbuk-gu, Seoul 02792, Republic of Korea. E-mail: wonchangchoi@kist.re.kr
[b]Division of Energy & Environment Technology, KIST School, Korea University of Science and Technology, Seoul 02792, Republic of Korea
[c]Department of Energy Engineering, Konkuk University, 120, Neungdong-ro, Gwangjin-gu, Seoul 05029, Republic of Korea
[d]Department of Chemical and Biological Engineering, Korea University, 145, Anam-ro, Sungbuk-gu, Seoul 02841, Republic of Korea

† Electronic supplementary information (ESI) available. See DOI: 10.1039/c8ta07854h

In this study, we report an intrinsic and comparative study of the thermal reactivity of fully charged Sn electrodes in SIB systems. To the best of our knowledge, there has hitherto been no comprehensive research work focused on the thermal properties of sodiated Sn electrodes, which are considered as promising candidates for next-generation battery systems such as SIBs. We also propose an effective strategy to limit the probability and damage of a thermal runaway event during SIB operation. An electrolyte additive is employed along with subsequent control to lower the energy generated at high temperatures and modify the thermal behavior of the SIB cells, resulting in the formation of an artificial surface passivation layer on the surface of the electrode material.

Experimental

Cell fabrication and electrochemical lithiation and sodiation measurements of the anode material

The Sn anode material was obtained from Sigma-Aldrich (<150 nm, Sigma-Aldrich). The anode was fabricated by blending a slurry of 85 wt% tin material, 7 wt% carbon black, and 8 wt% binder (poly (acrylic acid), molecular weight (M_v) = 350 000, Sigma-Aldrich) in ethanol. The blended slurry was cast on copper foil using a Doctor Blade coater, which had its height setting adjusted to 100 μm. The electrodes were dried at 120 °C in a vacuum oven for 24 h. The mass loading of the electrode was approximately 1.1–1.3 mg cm^{-2}. The coin cells were assembled in a glove box with 1 M $LiPF_6$ (Sigma-Aldrich), $NaPF_6$ (PANAX ETEC), and $NaClO_4$ (Sigma-Aldrich) in a mixture of ethylene carbonate (EC, Sigma-Aldrich), diethyl carbonate (DEC, Sigma-Aldrich) and propylene carbonate (PC, Sigma-Aldrich) (1 : 1 : 1 vol%) electrolytes. The introduction of fluoroethylene carbonate (FEC, PANAX ETEC) as an electrolyte additive was achieved by addition of 2 vol% FEC to the electrolyte previously described. A glass fiber filter (Whatman, UK) was used as a separator, and Li or Na metal was employed as the counter/reference electrode. The coin cells were assembled in a glove box, and the charge–discharge measurement was carried out in the voltage range of 1.2–0.001 V *versus* Li/Li^+ and 0.8–0.001 V *versus* Na/Na^+ at a rate of C/20 and C/5 to lithiate or sodiate the tin anodes at room (25 °C) temperature, respectively. The electrochemical impedance spectroscopy (EIS) measurements (VSP-300 potentiostat, Bio-logic Science Instruments) were carried out between 10 mHz and 1 MHz by applying an AC perturbation signal of 5 mV. The water content of the electrolyte was measured using a Mettler-Toledo coulometric KF titrator, model C20.

Materials characterization and DSC measurements

X-ray photoelectron spectroscopy (XPS) was conducted after the charge–discharge measurement, to further identify the chemical state and composition at the surface of the Sn electrode. Transmission electron microscopy (TEM) was acquired using Talos TEM (FEI; Talos F200X) operated at 200 keV to confirm the thickness of the SEI layer formed on the Sn electrode after cycling. The thermal stability of the Sn electrode was evaluated using differential scanning calorimetry (DSC, TA Instruments Auto Q20 instrument Auto Q20) with the fully lithiated or sodiated electrode. For the analysis, the lithiated or sodiated cells were disassembled in an argon-filled glove box and transferred into a bottle filled with dimethyl carbonate (DMC) to remove the electrolyte and residual salt from the anode material. After rinsing, the electrode was dried to remove the DMC solvent; it was then carefully scraped from copper foil for subsequent thermal analysis. To evaluate the thermal behavior of the Sn anodes using an electrolyte, 2 μl of the electrolyte and 1 mg of the lithiated or sodiated anode were introduced into stainless-steel high-pressure capsules and hermetically sealed to prevent any leakage of the pressurized electrolyte. All the samples were prepared inside a glove box in an argon atmosphere to prevent any possible contamination. The DSC profiles were obtained from 20 to 400 °C at a scan rate of 10 °C min^{-1}.

Results and discussion

Comparison of electrochemical and thermal behavior of a Sn electrode in LIB and SIB systems.

Electrochemical lithiation and sodiation of the Sn electrode were conducted before measuring the thermal stability of the electrode. EC : DEC : PC (1 : 1 : 1 vol%) was used as the solvent, and $LiPF_6$, which is presently the most widely used salt in commercial LIBs, was chosen as the lithium salt for the lithiation process.[40–45] Its electrochemical performance was compared to that of the Sn electrode in the SIB system using a $NaPF_6$ salt-based electrolyte. Fig. 1a compares the galvanostatic charge/discharge voltage profiles for the Sn electrode in the SIB and LIB by applying a constant current of 0.05 C-rate over three cycles. The charge/discharge voltages for both the Li and Na ions, show similar sequential stepwise potential plateaus. An initial lithiation/delithiation capacity of 974.2/751.0 mA h g^{-1} (corresponding to an initial coulombic efficiency of 77.1%) was achieved for the Sn electrode in the LIB system. In the SIB system, the Sn electrode showed a lower initial sodiation/desodiation capacity of 724.6/487.6 mA h g^{-1} (corresponding to an initial coulombic efficiency of 67.3%), compared to that of the LIBs. However, the reversible capacity of the Sn electrode in the SIB system increases and reaches approximately 701.8 mA h g^{-1} during the subsequent 2nd cycle, because of the activation of an electrochemical reaction for the electrode materials. These results indicate that the activation process of the Sn electrode in the SIBs is much slower than that in the LIBs because of the poor electrochemical sodiation/desodiation kinetics as the Na ions are approximately 55% larger in radius than the Li ions.[6,13,17,18] After the 3rd cycle, the Sn electrode in the SIB system exhibits drastic capacity fading (602.5 mA h g^{-1}), whereas the Sn electrode in the LIB system retains a high reversible capacity of 780.1 mA h g^{-1}. Fig. S1† compares the cycling performance of the Sn electrode in the SIB and LIB at 0.2C-rate during 50 cycles. The capacity retention *vs.* cycle number of both electrodes showed a similar behavior with severe capacity fading, but the Sn electrode in the LIB system (27.0%) exhibits slightly higher capacity retention than that of the Sn electrode in the SIB system (2.3%). As the alloying

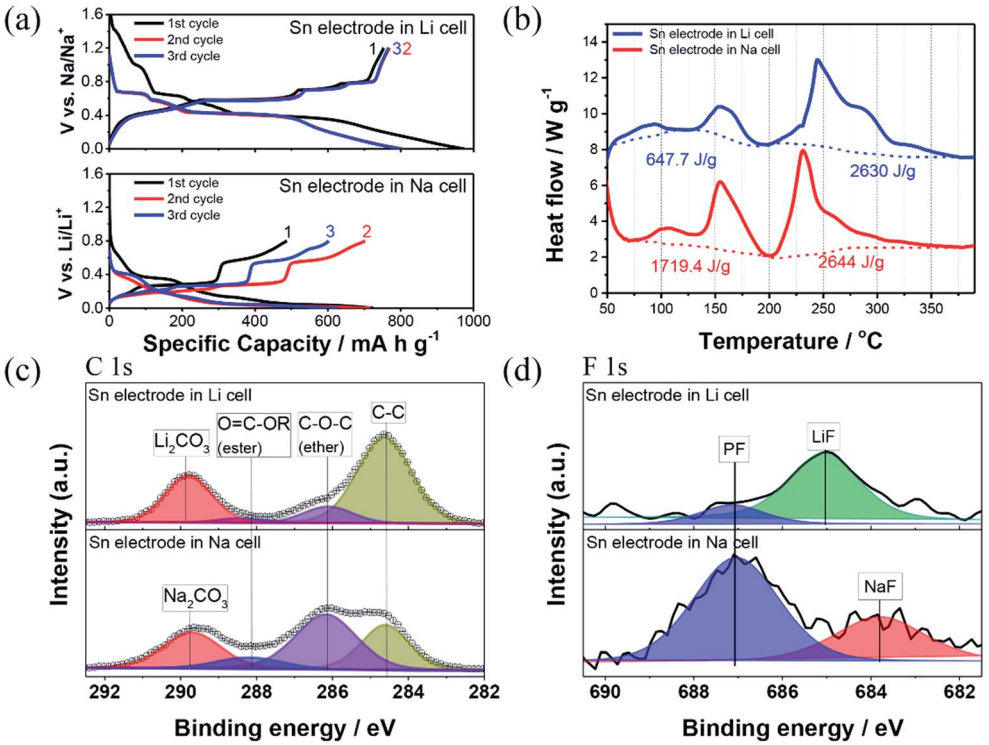

Fig. 1 (a) Voltage profiles of the Sn electrodes in a Li cell (using $LiPF_6$ salt) and Na cell (using $NaPF_6$ salt), (b) DSC profiles of the lithiated (using $LiPF_6$ salt) and sodiated Sn electrodes (using $NaPF_6$ salt) after three cycles. XPS (c) C 1s and (d) F 1s spectra for Sn electrodes in a Li cell and Na cell after three cycles.

reaction with Li or Na generally causes pulverization or cracking of particles, and subsequently results in the repetitive formation of a poorly conductive SEI layer. This implies that the Sn electrode in the $NaPF_6$-based electrolyte system undergoes more chemical or mechanical degradation during sodiation/desodiation than that in the LIB system, and consequently exhibits severe capacity fading.[18,19,32–34] Furthermore, the thermal reactions between the fully charged anodes and the electrolytes are crucial for battery safety because the thermal decomposition of the SEI layer on the anode surface is initiated in the battery system.[46–48] As shown in Fig. 2, the SEI layer on the anode generally breaks down/cracks at a temperature of approximately 100 °C, and further chemical reactions then occur between the SEI-free anode and the electrolyte, leading to the repetitive and unwanted formation of an SEI layer on the anode materials during battery operation. Subsequently, the thermal decomposition of the secondary SEI layer occurs, resulting in thermal reactions with the binder, which generates additional heat.[46–48] Therefore, the electrochemical behaviors shown in Fig. 1a indicate that a stable SEI layer does not form readily on the anode surface of the SIBs compared to that of the LIBs.

In general, the fully-charged anodes without electrolytes are known to be thermally stable.[44] As demonstrated in Fig. S2a,† the Sn electrode without electrolytes in the sodiated state did not produce any considerable exothermic peaks. On the other hand, the electrolyte alone is known to undergo an exothermic reaction due to their thermal decomposition and flammability. In Fig. S2b,† 1 M $NaClO_4$ in the EC : DEC : PC electrolyte alone, which is mainly used in this study, gave exothermic heat generation at a temperature higher than 260 °C, which was caused by the thermal decomposition of the electrolytes. The thermal stability of the electrolytes is dominated by the salts and solvents. The Okada group tested the various Li and Na salts in different electrolyte solvent mixtures already in 2013, and they concluded that the Na-salt electrolytes had better thermal stability than their Li-salt electrolyte counterparts, and the EC : The DMC-based electrolytes have better thermal stability than the PC-based ones.[25] In this regard, the thermal properties of the coexisting system of fully-charged Sn electrodes with Li- and Na-based electrolytes must be systematically investigated.

To examine and compare the thermal behavior of the fully lithiated or sodiated Sn electrode to a hexafluorophosphate-based electrolyte, the DSC experiments were carried out (Fig. 1b). In brief, the lithiated and sodiated Sn electrodes with the hexafluorophosphate-based electrolytes show similar trends in thermal properties. These consist of the first mild exothermic heat at 50–200 °C because of the thermal decomposition reaction of the SEI layer. The second exothermic heat then occurs at higher temperatures corresponding to the direct reaction between the charged electrode and the electrolyte during operation.[28,42–48] A similar thermal reaction pattern is observed for both the fully lithiated and sodiated Sn electrodes whereas the lithiated Sn electrode in the $LiPF_6$-based electrolyte clearly shows a lower exothermic heat generation of 647.7 J g^{-1}

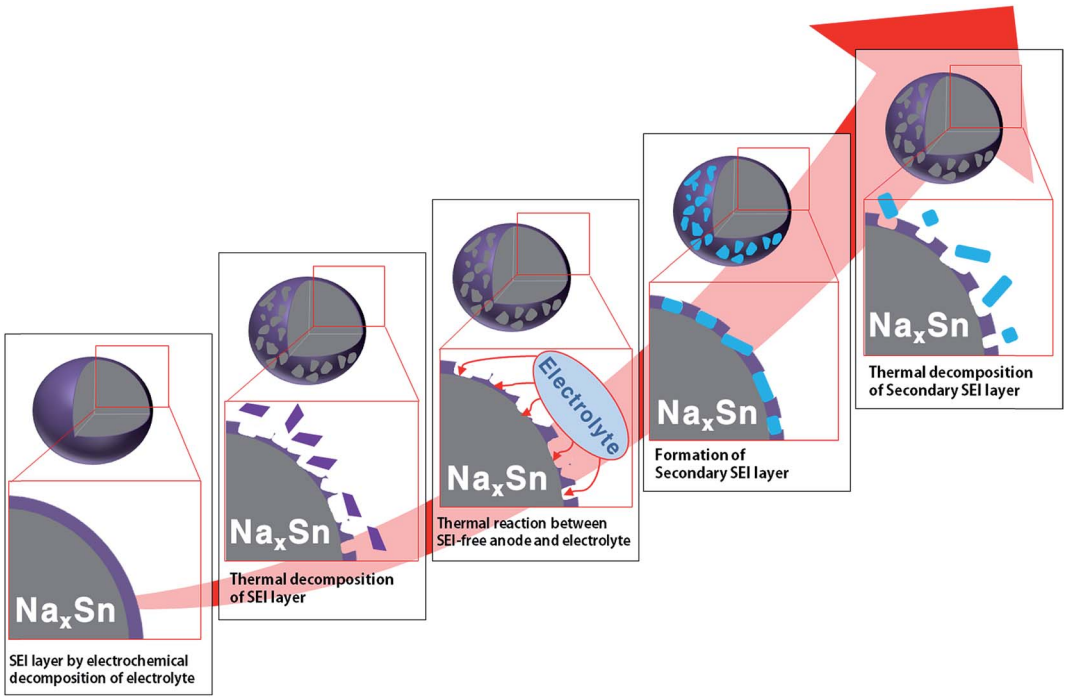

Fig. 2 Schematic diagram showing the thermal events in the fully sodiated Sn electrode with electrolyte.

corresponding to the thermal decomposition reaction of the SEI layer, as compared to that of the sodiated Sn electrode in the $NaPF_6$-based electrolyte (1719.4 J g^{-1}). A comparison of the second exothermic heat values, which correspond to the direct reaction between the charged electrode and electrolyte, revealed that the Sn electrodes in both battery systems exhibit a similar heat generation value (lithiated Sn electrode: 2630 J g^{-1} and sodiated Sn electrode: 2644 J g^{-1}), but the second exothermic peak of the sodiated Sn electrode occurs at lower temperatures compared to that of the lithiated Sn electrode. This suggests that thermally unstable and thicker SEI layers formed on the surface in the case of the sodiated Sn electrode because of the greater decomposition of the $NaPF_6$-based electrolyte, and thermal decomposition of the unstable SEI layers on the Sn electrode in the SIB system accelerates further thermal reactions between the SEI-free anode and the electrolyte. The thermally unstable SEI layer and consequent exothermic heat values caused by the thermal decomposition reaction of the SEI layer on the anode side is considered to be the most critical factor influencing the overall thermal stability in a practical full-cell assembly. This is because the heat accumulated during the first exothermal reaction raises the internal temperature of the cell and eventually triggers a runaway thermal reaction between the cathode and electrolyte.[28,42–48] Therefore, the DSC results shown in Fig. 1b indicate that the Sn electrode in the SIB system was less thermally stable than that in the LIB system.

As the components and quantity of the SEI layer decomposed *via* electrochemical reaction of the electrolyte mainly influence the thermal stability of the anode, the surface chemical components of the Sn electrodes cycled in the $LiPF_6$- and $NaPF_6$-based electrolytes were analyzed using XPS to identify and understand the thermal influence of the two battery systems on the surface properties of the Sn electrode. As shown in Fig. 1c, a comparative XPS spectra of the Sn electrode revealed similar compounds for both the LIB and SIB cells; a peak at 284.6 eV in the C 1s XPS spectra is assigned to conductive carbon, and the other peaks originate from the decomposition of the electrolyte components (C–O–C at 286.0, O=C–OR at 288.1 eV, and $LiCO_3$/Na_2CO_3 at 289.4 eV).[7,14,18,19,28,44,49] However, in the case of the Sn electrode cycled in the $NaPF_6$-based electrolyte, the intensity of the peak corresponding to the C–C bond of carbon black discernibly decreases, and the peaks assigned to ether (C–O–C) intensifies, as compared to the Sn electrode cycled in the LIB system. In the F 1s spectra, the Sn electrodes in both battery systems showed that upon cycling the slight emergence of two peaks at 684/685 and 687 eV correspond to the NaF/LiF and P–F species, respectively, which was ascribed to the electrochemical reduction of the $LiPF_6$ or $NaPF_6$ salts in the electrolyte.[10,18,19,40,44] Interestingly, the peak assigned to the P–F bond is more intense in the case of the Sn electrode cycled in the $NaPF_6$-based electrolyte, compared to that in the LIB system. To confirm the thickness of the SEI layers formed on the surface of the Sn electrodes in both battery systems, TEM analysis was carried out. From the TEM observation as shown in Fig. S3,† the surface film formed on the Sn electrode in the SIB system has a thickness of approximately 9.9 nm, which is 2 times thicker than that of the Sn electrode in the LIB system (4.4 nm). From these results, we can conclude that the thicker surface film formed on the Sn electrode because of the severe electrochemical decomposition of the $NaPF_6$-based electrolyte compared to that of the $LiPF_6$-based electrolyte, which is consistent with the electrochemical data concerning the lower initial coulombic efficiency

and the reversible capacity as shown in Fig. 1a.[18] These XPS and TEM results also explain the thermal reaction observed of a much greater and more drastic heat generation during the first exothermic reaction for the sodiated Sn electrode/$NaPF_6$-based electrolyte system, as shown in Fig. 1b.

Comparison of the electrochemical and thermal behavior of the Sn electrode cycled in a $NaClO_4$- and $NaPF_6$-based electrolyte

Although the $NaPF_6$-based electrolyte, which is analogous to the $LiPF_6$ salt in the LIB system, has an advantage because of the easy removal of water contents by vacuum drying, a highly purified $NaPF_6$ salt is needed to obtain an electrolyte of high concentration, as compared to the $NaClO_4$-based electrolyte system.[1] For this reason, more than two-thirds of the previous literature has employed $NaClO_4$-based electrolytes.[1] Furthermore, there are no comprehensive studies concerning the comparison of the electrochemical and thermal stability of the anodes between the $NaPF_6$- and $NaClO_4$-based electrolyte systems to the best of our knowledge. Fig. 3a exhibits the voltage potential *versus* capacity profile for a Sn electrode during the 1st cycle using a 1 M solution of $NaClO_4$ in EC : DEC : PC as the electrolyte in comparison to that of a Sn electrode in a 1 M solution of $NaPF_6$ in EC : DEC : PC as the electrolyte. While both Sn electrodes exhibit similar electrochemical behaviors with the stepwise potential plateaus in the first discharge/charge curves, a slightly lower over-potential value between discharge and charge was observed for the Sn electrode in the $NaClO_4$-based electrolyte system, as compared to that in the $NaPF_6$-based electrolyte system (inset in Fig. 3a). In addition, the Sn electrode in the $NaClO_4$-based electrolyte system delivers a higher capacity of 547.8 mA h g^{-1} and has a coulombic efficiency of 75.2% as compared to that of the Sn electrode in the $NaPF_6$-based electrolyte (487.6 mA h g^{-1} and 67.3%). The differential capacity *versus* voltage (dQ/dV) curves during the 1st cycle as shown in Fig. 3b also clearly indicate that the cathodic and anodic peaks of the Sn electrode in the $NaPF_6$-based electrolyte shifted towards the lower and higher potential positions, which suggests that the polarization increased on the surface of the Sn electrode when the $NaPF_6$ salt was used instead of $NaClO_4$ as the electrolyte salt component largely because of the less conductive and/or thicker SEI layer.[25,26] To understand the influence of sodium salts on the SEI resistance, the EIS of the Sn electrodes cycled in the $NaClO_4$- and $NaPF_6$-based electrolytes after 3 cycles was carried out; the Nyquist plots of the EIS measurements are shown in Fig. S4a.† The impedance spectra are fitted by the equivalent circuit diagram given in Fig. S4b,† and the numerical values obtained from the fitting process are shown in Table S1.† All the plots consist of a depressed semicircle in the high to medium frequency region, and a sloping line in the low frequency region. The depressed semicircle consists of two partially overlapping semicircles. The first semicircle relates to the transport of Na ions through the SEI film, and the second one corresponds to the charge transfer reactions, while the sloping line corresponds to the diffusion of Na ions in the bulk material.[19] The $R_{electrolyte}$ is electrolyte resistance, R_{SEI} and CPE_{SEI} are the SEI film resistance and the relax capacitance, R_{CT} and CPE_{CT} denote the charge transfer

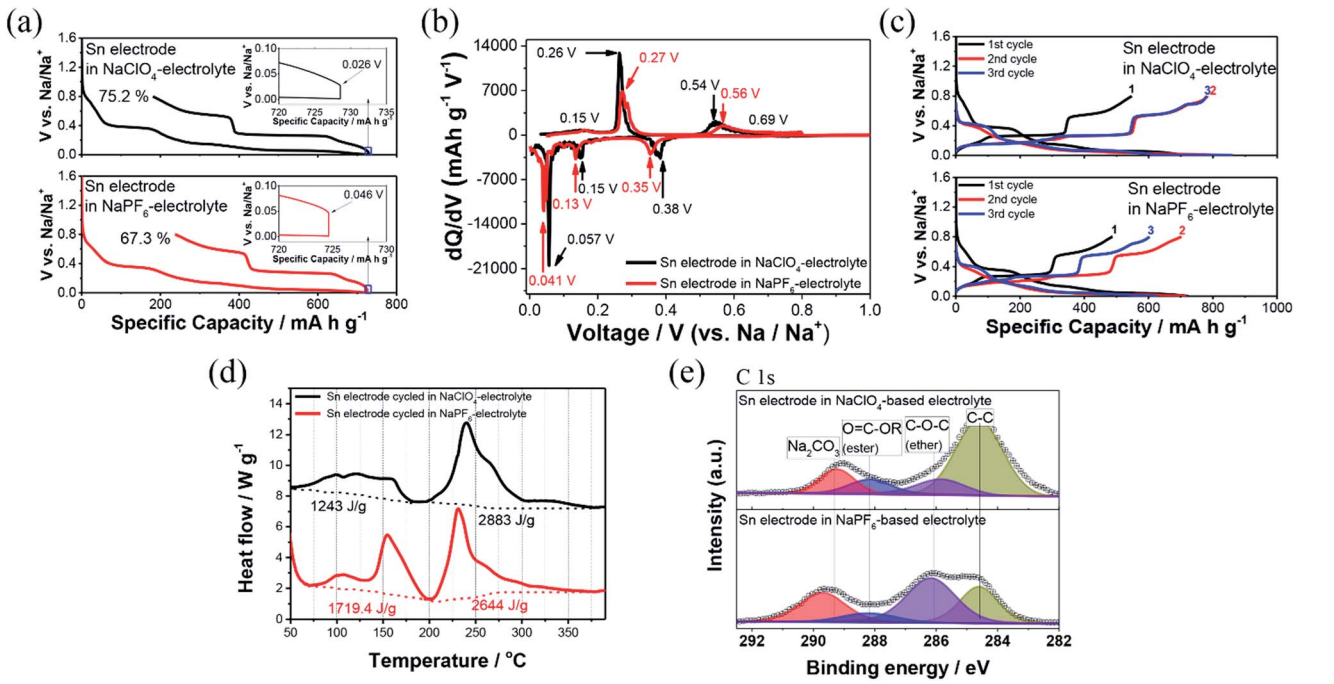

Fig. 3 Comparison of the electrochemical and thermal behavior for the Sn electrode in the $NaClO_4$- and $NaPF_6$-based electrolytes. (a) 1st cycle voltage *versus* specific capacity profile. (the inset in (a) indicates overpotential of the Sn electrodes in the two electrolyte systems), (b) dQ/dV profiles during the initial cycle, and (c) voltage *versus* specific capacity profiles during the initial three cycles, (d) DSC profiles of the sodiated Sn electrodes after three cycles, (e) XPS C 1s spectra of the Sn electrodes after three cycles.

resistance and the double layer capacitance, and Z_w is the bulk diffusion resistance.

Although the electrolyte resistance for both electrodes remains similar, the Sn electrode cycled in the $NaPF_6$-based electrolyte exhibits R_{SEI} and R_{CT} values of 70.0 and 231.4 Ω, respectively, which is higher than those of the Sn electrode cycled in the $NaClO_4$-based electrolyte (R_{SEI}: 25.1 Ω, R_{CT}: 94.4 Ω), indicating that the less conductive SEI layer formed on the surface of the Sn electrode when the $NaPF_6$ salt was used instead of the $NaClO_4$ salt. Furthermore, these EIS analysis results also explain the increase of the polarization on the surface of the Sn electrode cycled in the $NaPF_6$-based electrolyte, as observed in Fig. 3a and b.

As shown in Fig. 3c, the reversible capacity of the Sn electrode using an $NaClO_4$-based electrolyte increases and reaches a value of approximately 780.1 mA h g^{-1} because of the activation of the electrode during the 2nd cycle, and the high reversibility which remained during the following 3rd cycle, whereas the Sn electrode using the $NaPF_6$-based electrolyte exhibits continuous capacity fading during the three cycles. This phenomenon reflects the continuous growth of the poorly conductive SEI layer during cycling, and this result is consistent with previous studies, which showed that the $NaPF_6$-based electrolyte could promote the formation of a copious and poorly conductive SEI layer at the surface of the hard carbon electrode compared to the $NaClO_4$-based electrolyte.[25,26] In Fig. S1,† the cycling performance of the Sn electrode between the $NaPF_6$- and $NaClO_4$-based electrolyte systems was compared at 0.2C-rate during 50 cycles. The desodiation capacity of both electrodes decreases rapidly, indicating that the cyclability of the Sn electrode is not improved by using $NaClO_4$ as salts of the electrolyte instead of $NaPF_6$ due to the large volume changes of the Sn materials during cycling.

To compare the thermal behavior between the $NaPF_6$- and $NaClO_4$-based electrolytes for the fully sodiated Sn electrode, the DSC experiments were carried out, as shown in Fig. 3d. In the temperature range of 50–200 °C, the Sn electrode for the $NaClO_4$-based electrolyte system exhibited a heat generation of approximately 1243 J g^{-1} whereas the Sn electrode in the $NaPF_6$-based electrolyte exhibited an increased heat generation of approximately 1719.4 J g^{-1} originating from the thermal decomposition reaction of the SEI layer. In contrast, the Sn electrodes in both electrolyte systems showed nearly equivalent heat generation ($NaClO_4$-based electrolyte system: 2644 J g^{-1} and $NaPF_6$-based electrolyte system: 2883 J g^{-1}) during the second exothermic reaction, but the exothermic peak of the Sn electrode for the $NaClO_4$-based electrolyte system occurs at higher temperatures compared to that of the Sn electrode for the $NaPF_6$-based electrolyte system corresponding to the direct reaction between the sodiated Sn and electrolyte. These results indicate that the large SEI-free area on the Sn electrode for the $NaPF_6$-based electrolyte system is more exposed to the electrolytes by the thermal decomposition reaction of the SEI layer, resulting in the acceleration of further thermal reactions between the SEI-free anode and the electrolyte. Notably, the sodiated Sn electrode in the $NaClO_4$-based electrolytes showed a drastic decrease in heat generation by approximately 72% particularly during the first exothermic reaction corresponding to the thermal decomposition reaction of the SEI layer, compared to the sodiated Sn electrode in the $NaPF_6$-based electrolytes. As the first exothermic reaction in the low temperature range significantly influences the subsequent reaction of both the cathode and anode in the case of a practical full cell, these results indicate that thermally stable or thinner SEI layers are formed on the surface of the Sn electrode cycled in the $NaClO_4$-based electrolytes compared to those on the Sn electrodes cycled in the $NaPF_6$-based electrolytes.[42–48]

To identify and understand the surface chemical components of the SEI layer, the XPS analyses were conducted, and the XPS spectra obtained were compared as shown in Fig. 3e. The XPS C 1s spectra of the Sn electrode cycled in the $NaClO_4$-based electrolyte shown in Fig. 3e reveals that similar compounds (C–C at 284.6 eV, C–O–C at 286.0, O=C–OR at 288.1 eV, and CO_3 at 289.8 eV) concerning SEI films were formed, as compared to those of the Sn electrode cycled in the $NaPF_6$-based electrolyte. However, it is noticeable that the proportions differ with a significantly smaller number of organic compounds (C–O–C) for the Sn electrode cycled in the $NaClO_4$-based electrolytes. The intensity of the peak corresponding to the C–C bond of carbon black significantly increased, as compared to that of the Sn electrode cycled in the $NaPF_6$-based electrolytes. From the TEM images collected after 3 cycles as shown in Fig. S3,† the surface film formed on the Sn electrode in the $NaClO_4$-based electrolyte has a thickness of approximately 7.5 nm, which is slightly thinner than that on the Sn electrode in the $NaPF_6$-based electrolyte (9.9 nm). These results indicate that a thinner surface film formed on the Sn electrode *via* the decomposition of the $NaClO_4$-based electrolyte compared to that of the $NaPF_6$-based electrolyte, which is consistent with the electrochemical results such as the higher coulombic efficiency and smaller polarization as well as the suppressed heat generation during the first exothermic peak during the DSC experiment in the case of the sodiated Sn electrode in the $NaClO_4$-based electrolyte system.

Electrochemically and thermally stable artificial SEI layer formation on the surface of the Sn electrode *via* electrolyte additive

It was reported that the FEC additive reductively decomposes on the anode surface at a higher potential than other organic solvents such as EC, DEC, and PC, and provides a uniform surface film for the electrochemical stability of the anode.[14,18,32,43,44,49] Previously, many researchers reported that FEC as an additive generating an electrochemically stable and thin SEI layer drastically improved the electrochemical properties of an alloy-based electrode in a SIB system.[14,18,32,43,49] However, there are few publications describing the role of FEC additives on the thermal behaviors of anodes at elevated temperatures for SIBs. Hence, we report the influence of an FEC additive on the thermal properties of the Sn electrode in this section.

As the FEC additives are known to influence the formation of the SEI film during the initial electrochemical operation, the electrochemical sodiation of the Sn electrode in the FEC-containing electrolyte was preliminarily conducted. Fig. 4a

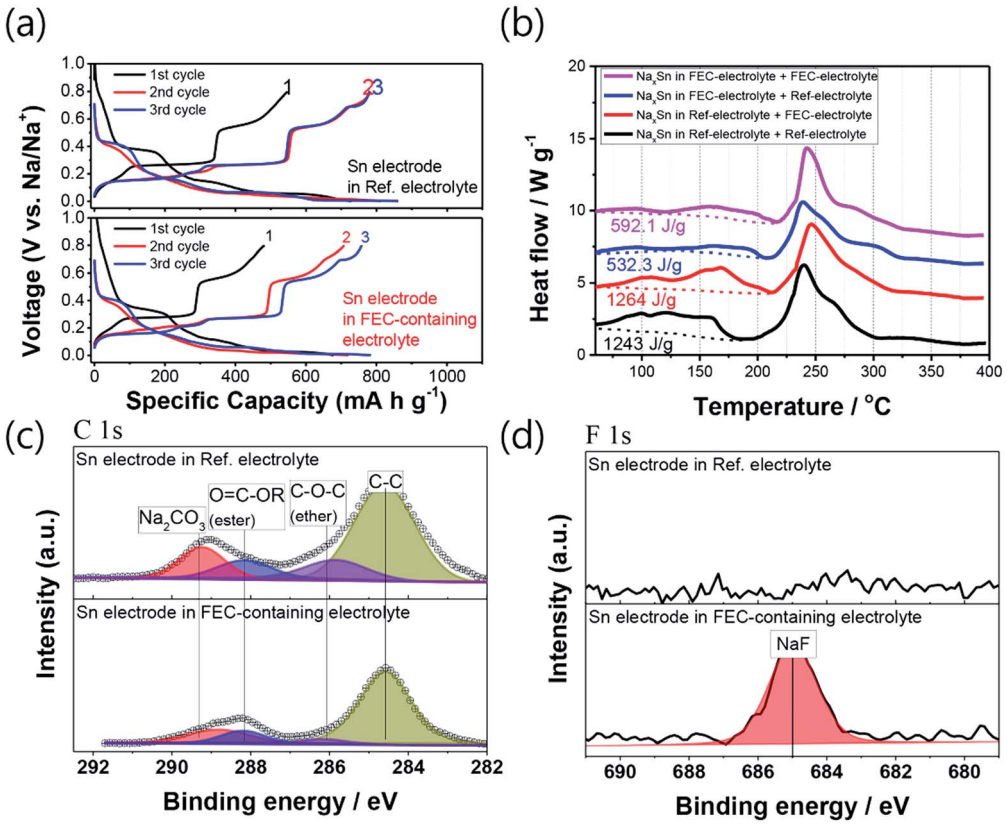

Fig. 4 (a) Voltage profiles of the Sn electrode during the initial three cycles and (b) DSC profiles of the sodiated Sn electrode after three cycles. XPS (c) C 1s and (d) F 1s spectra for the Sn electrodes after three cycles in the $NaClO_4$-based electrolytes with/without 2 vol% FEC additives.

illustrates the typical voltage profiles obtained for the Sn electrode cycled in the $NaClO_4$-based electrolyte with or without the FEC additives during three cycles. A slight diminution of the specific charge/discharge capacity was observed for the Sn electrode in the FEC-containing electrolyte possibly because of the additive decompositions during three cycles;[44] however, the highest coulombic efficiency of 96.7% was obtained in the FEC-containing electrolyte after activation of three cycles, compared to that of the pristine electrolyte (90.5%). Fig. S1† compares the cycling performance of the Sn electrode in the $NaClO_4$-based electrolyte systems with and without the FEC additive at 0.2C-rate during 50 cycles. The Sn electrode with the FEC additive showed excellent capacity retention of 87.9% without capacity degradation as observed for the electrolyte without FEC, indicating that FEC generates an electrochemically stable surface film, permitting the reversible sodiation of sodium ions into Sn materials without any harmful influence during battery operation.[14,18,32,43,49]

As the FEC additive may influence the thermal reaction with the Sn electrode during the DSC experiment, in addition to the formation of the SEI film during the electrochemical reaction, we prepared four different samples to separate the previously mentioned influence and investigate the thermal stability of the sodiated Sn electrode with the FEC-containing electrolytes. For example, a sample, denoted as Na_xSn in the Ref-electrolyte + FEC-electrolyte in Fig. 4b, represents that the Sn electrode was initially cycled in an electrolyte without an FEC additive system, and then the DSC experiment was carried out with a mixture of the Sn electrode and the electrolyte including the FEC additives. As shown in Fig. 4b, a comparison of the second exothermic heat values, corresponding to the direct reaction between the charged electrode and electrolyte, revealed that the Sn electrodes in both electrolyte systems exhibit a similar heat generation value (FEC + FEC: 2510 J g^{-1}, Ref + Ref: 2644 J g^{-1}). However, the amount of heat generated in the region between 50 and 200 °C corresponding to the thermal decomposition of the SEI layer is markedly reduced for the sodiated Sn electrode cycled in the FEC-containing electrolyte (592.1 J g^{-1}), compared to that of the sodiated Sn electrode without FEC (1243 J g^{-1}). This result indicates that SEI layers derived from an FEC-containing electrolyte prevent the thermal degradation of the sodiated Sn electrode. In this regard, there are several possible mechanisms for thermal protection of the sodiated Sn electrodes using FEC additives at elevated temperatures; (i) the formation of a thermally resistive SEI layer during the first sodiation *via* electrochemically reductive decomposition of the FEC additives and (ii) the generation of a protective film on the electrode surface *via* thermal degradation of the FEC additives during heating.[43] Therefore, to separate and elucidate the role of the FEC additives, the DSC measurements were conducted (i) for the Sn electrode, which is sodiated in the FEC-containing electrolyte, and then heated with the pristine electrolyte (denoted as FEC + Ref system); or (ii) for the Sn electrode, which is sodiated in the pristine electrolyte, and then heated with the FEC-containing electrolyte (denoted as Ref + FEC system).

A comparison of the second exothermic heat values revealed that the Sn electrodes in both electrolyte systems also exhibited similar heat generation values (FEC + Ref: 2578 J g^{-1}, Ref + FEC: 2518 J g^{-1}). In contrast, the remarkably reduced heat generation in the region between 50 and 180 °C corresponding to the thermal decomposition of the SEI layer was observed in the Na_xSn in the FEC + Ref system (532.3 J g^{-1}), which is similar to that of the sodiated Sn electrode in the FEC + FEC system, while the sodiated Sn electrodes in the Ref + FEC system still exhibited a high heat generation value *via* the thermal decomposition reaction of the SEI layer (1264 J g^{-1}). From these results, we can conclude that the formation of a thermally protective SEI layer employing FEC additives during the initial electrochemical operation plays an important role in thermal stability, as compared to the decomposition of an FEC additive itself during the DSC experiment.

To obtain information on the surface composition of the SEI layer of a Sn electrode under the influence of electrochemically reductive decomposition of FEC additives, XPS analysis was conducted as shown in Fig. 4c and d. In the C 1s spectra of the Sn electrode cycled in the FEC-containing electrolyte, except for their peak intensities, there were no significant differences, compared to those of the Sn electrode cycled in the pristine electrolyte. Interestingly, the Sn electrode cycled in the FEC-containing electrolyte exhibited much reduced peak intensities in organic compounds, corresponding to carbonate, ester, and ether, compared to those of the Sn electrode cycled in the pristine electrolyte. This result indicated that the formation of the organic surface film on the anode surface was suppressed because of the electrochemical decomposition of the FEC additive at a higher potential than the other organic solvents such as EC, DEC and PC, which means that the FEC relation to the SEI film formed earlier.[44] This explains why the FEC additive is so effective in enhancing the coulombic efficiency.[2,14,43,44] In the F 1s spectra as shown in Fig. 4d, the presence of NaF is clearly observed at 685.0 eV for the Sn electrode cycled with the FEC additive because of its electrochemical decomposition, while no peaks were observed for the Sn electrode cycled in the pristine electrolyte. As it is known that NaF is a thermally stable inorganic solid at high temperatures,[27,30] we believe that the formation of NaF improves the thermal stability of the SEI layer on the surface of the sodiated Sn electrode, and thus the addition of FEC in an electrolyte decreases the thermal decomposition reaction of the sodiated Sn electrode with the electrolyte at a low temperature.

Effect of FEC additive on the thermal stability of sodiated Sn electrode cycled with a water-containing electrolyte

It was reported that the addition of water to a $LiPF_6$-based electrolyte with anodes accelerates the exothermic reaction because of a collapse in the SEI layer in response to HF and POF_3, which is a product of the reaction between the added water and PF_5 dissociated from the $LiPF_6$ salt.[41,50–52] In this regard, as the $NaClO_4$ salt generally used in the SIB system does not include fluorophosphate-based molecules, it is expected that the residual water in the $NaClO_4$-based electrolyte may not significantly influence the electrode materials, although the previous literature has not addressed this point thus far to the best of our knowledge. In this section, we conducted experiments to investigate whether or not the residual water in the $NaClO_4$-based electrolyte would influence the electrochemical and thermal properties of the Sn electrode. As shown in Fig. 5, the galvanostatic charge/discharge measurements and the DSC measurements for a Sn electrode with a water-containing electrolyte were investigated, and they were compared to the electrochemical and thermal behavior of a Sn electrode with a pristine electrolyte as shown in Fig. 3c. Table 1 shows the water contents of the pristine electrolyte (P-electrolyte, not exposed to the atmospheric environment) and a water-containing electrolyte (W-electrolyte, which is exposed to a humidity of 43% in an atmospheric environment, at 25 °C for 2 h). The water content of the electrolyte, which is exposed to

Table 1 Water contents of pristine electrolyte and water-containing electrolyte

Electrolyte: 1 M $NaClO_4$/EC : DEC : PC	Aging time in air (h)	Water content (ppm)
Pristine electrolyte (P-electrolyte)	0	18.3
Water containing electrolyte (W-electrolyte)	2	517.6

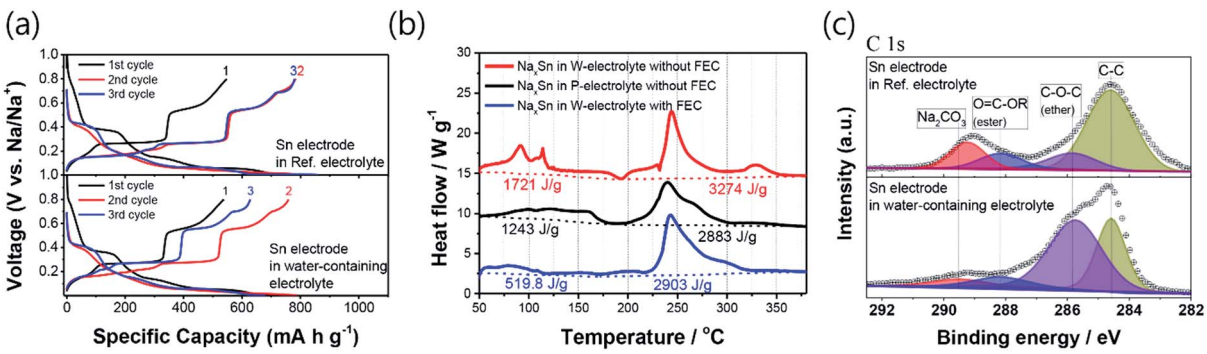

Fig. 5 (a) Voltage profiles of a Sn electrode during the initial three cycles and (b) DSC profiles of the sodiated Sn electrode after three cycles. (c) XPS F 1s spectra for Sn electrodes in the $NaClO_4$-based electrolytes after three cycles in the $NaClO_4$-based electrolytes with/without water contents.

a humidity of 43% in an atmospheric environment, was approximately 517.6 ppm, which was approximately 28 times greater than that of the pristine electrolyte (18.3 ppm). As shown in Fig. 5a, the Sn electrode with the W-electrolyte had similar discharge/charge capacities during the initial two cycles with a similar coulombic efficiency of approximately 75% (1st cycle) and 96% (2nd cycle), respectively, compared to those of the Sn electrode with the P-electrolyte. However, the Sn electrode with the W-electrolyte showed a rapid capacity fade to 681.1 mA h g^{-1} (discharge capacity) and 628.2 mA h g^{-1} (charge capacity) during the 3rd cycle, while the Sn electrode with the P-electrolyte showed negligible capacity fading. In Fig. S1,† the desodiation capacity of the Sn electrodes with the W-electrolyte during 50 cycles at 0.2C-rate decreases more rapidly, compared to that of the Sn electrode with the P-electrolyte, indicating that the undesirable electrochemical reaction of the Sn electrode in the W-electrolyte occurred during cycling. The thermal behavior of the Sn electrode, which is fully sodiated in the W-electrolyte, was also investigated as shown in Fig. 5b. Two sharp exothermic peaks corresponding to the thermal decomposition of the SEI layer with a heat generation of 1721 J g^{-1}, and a second exothermic reaction with enormous heat generation of approximately 3274 J g^{-1}, higher than the pristine system, indicate that water is undesirable for the thermal behavior of the Sn electrode in the SIB system. From the results shown in Fig. 5a and b, it can be assumed that a thicker surface film or undesirable surface species formed on the Sn electrode *via* a side reaction of water in the electrolyte.

XPS analysis was conducted as shown in Fig. 5c to identify and understand the surface chemical components of the Sn electrodes cycled in the W-electrolyte. The C 1s spectra of the Sn electrodes cycled in the W-electrolytes showed similar SEI compositions, compared to those of the Sn electrodes cycled in the P-electrolytes. However, it is noticeable that the proportions differ with a significantly larger number of organic compounds (C–O–C) in the Sn electrode cycled in the W-electrolyte, and the intensity of the peak corresponding to the C–C bond of carbon black discernibly decreases, compared to the Sn electrode in the P-electrolyte. This indicates that a thicker surface film formed *via* the undesirable side reaction of the W-electrolyte compared to the P-electrolyte, which is consistent with the results of the electrochemical test observation showing the lower coulombic efficiency (Fig. 5a) as well as the thermal reaction observed with a much greater and more drastic heat generation during the first exothermic reaction of the mixture of the sodiated Sn electrode in the W-electrolyte as shown in Fig. 5b. These results indicate that an organic solvent with water may experience severe decomposition during cycling. The Palacin group reported that a significant increase in the amount of C–O was observed when EC was present in the electrolyte, which was attributed to the ring opening of EC with the formation of polyethylene oxide (oligomeric/polymeric species) and CO_2 evolution,[1] which may have participated in the SEI decomposition reaction at high temperature. The ring-opening reaction of EC is more commonly activated when water is present in the electrolyte,[53,54] resulting in the largest number of SEI layers and a more exothermic reaction contributing to the thermal reactivity of the SEI. In the case of the peak concerning the Na_2CO_3 component, a very weak peak was observed for the Sn electrode cycle in the W-electrolyte possibly because of the water-soluble characteristics of the Na_2CO_3 materials.[14,31]

To examine the effect of the FEC additive or the consequent formation of a NaF-containing SEI film layer on the anode materials in the presence of water, a DSC experiment was also performed, and the DSC result is shown in Fig. 5b. Surprisingly, the intensity of the exothermic peaks contributing to the thermal decomposition of the SEI layer below 180 °C is prominently suppressed, and the heat generation is also remarkably reduced in the presence of FEC (519.8 J g^{-1}), indicating that the FEC additive even enhances the thermal stability of the Sn electrode in spite of the presence of water in the electrolyte. As previously described, the FEC additive acts as a film-formation additive to build a more stable interphase between the anode and electrolyte, which protects the thermal decomposition of the SEI layer from direct contact with the electrolyte solution and reduces the exothermic reaction.

Conclusions

The safety risk of a fully sodiated Sn electrode was intensively evaluated using a DSC instrument in a temperature range from 20 to 400 °C. For comparison, the thermal behavior of a lithiated Sn electrode was also tested with a counterpart electrolyte. Based on the DSC results, the $NaPF_6$-based electrolyte yielded the formation of a thicker surface film on the Sn electrode, leading to an intense thermal decomposition reaction of the SEI layer, compared to that of the lithiated Sn electrode. In addition, the $NaPF_6$-based electrolyte yielded a slightly less conductive and/or thicker SEI layer than the $NaClO_4$-based electrolyte, resulting in a lower coulombic efficiency, an intense polarization increase, and a thermal reaction of drastic heat generation, compared to that of the $NaClO_4$-based electrolyte. The important role of the FEC additive in the thermal stabilization of the sodiated Sn electrode with the electrolyte was also confirmed because of the formation of NaF in the SEI, which effectively restrained the exothermic reaction contributing to the thermal reactivity of the SEI.

Conflicts of interest

There are no conflicts to declare.

Acknowledgements

This work was supported by the Basic Science Research Program through the National Research Foundation of Korea (NRF) funded by the Ministry of Science and ICT (No. 2018R1A2B2007081).

Notes and references

1 A. Ponrouch, D. Monti, A. Boschin, B. Steen, P. Johansson and M. R. Palacín, *J. Mater. Chem. A*, 2015, **3**, 22.
2 K. Vignarooban, R. Kushagra, A. Elango, P. Badami, B.-E. Mellander, X. Xu, T. G. Tucker, C. Nam and A. M. Kannan, *Int. J. Hydrogen Energy*, 2016, **41**, 2829.
3 V. Palomares, P. Serras, I. Villaluenga, K. B. Hueso, J. Carretero-González and T. Rojo, *Energy Environ. Sci.*, 2012, **5**, 5884.
4 M. D. Slater, D. Kim, E. Lee and C. S. Johnson, *Adv. Funct. Mater.*, 2013, **23**, 947.
5 M. S. Islam and C. A. Fisher, *Chem. Soc. Rev.*, 2014, **43**, 185.
6 H. Pan, Y.-S. Hu and L. Chen, *Energy Environ. Sci.*, 2013, **6**, 2338.
7 V. Palomares, M. Casas-Cabanas, E. Castillo-Martínez, M. H. Han and T. Rojo, *Energy Environ. Sci.*, 2013, **6**, 2312.
8 Y. Wang and J. R. Dahn, *J. Electrochem. Soc.*, 2006, **153**, A2188.
9 Y. S. Yun, J. H. Kim, S.-Y. Lee, E.-G. Shim and D.-W. Kim, *J. Power Sources*, 2011, **196**, 6750.
10 L. El Ouatani, R. Dedryvère, C. Siret, P. Biensan, S. Reynaud, P. Iratçabal and D. Gonbeau, *J. Electrochem. Soc.*, 2009, **156**, A103.
11 Q. Wang, J. Sun, X. Chen, G. Chu and C. Chen, *Mater. Res. Bull.*, 2009, **44**, 543.
12 K. B. Hueso, M. Armand and T. Rojo, *Energy Environ. Sci.*, 2013, **6**, 734.
13 I. Hasa, R. Verrelli and J. Hassoun, *Electrochim. Acta*, 2015, **173**, 613.
14 M. Dahbi, N. Yabuuchi, K. Kubota, K. Tokiwa and S. Komaba, *Phys. Chem. Chem. Phys.*, 2014, **16**, 15007.
15 Z. Hu, Q. Liu, S.-L. Chou and S.-X. Dou, *Adv. Mater.*, 2017, **29**, 1700606.
16 F. Klein, B. Jache, A. Bhide and P. Adelhelm, *Phys. Chem. Chem. Phys.*, 2013, **15**, 15876.
17 W.-H. Ryu, H. Wilson, S. Sohn, J. Li, X. Tong, E. Shaulsky, J. Schroers, M. Elimelech and A. D. Taylor, *ACS Nano*, 2016, **10**, 3257.
18 J. Y. Jang, Y. Lee, Y. Kim, J. Lee, S.-M. Lee, K. T. Lee and N.-S. Choi, *J. Mater. Chem. A*, 2015, **3**, 8332.
19 Y. Lee, K. Y. Lee and W. Choi, *Adv. Funct. Mater.*, 2017, **27**, 1702607.
20 Y. Fang, X. Y. Yu and X. W. Lou, *Adv. Mater.*, 2018, **30**, 1706668.
21 X.-W. Lou, *Angew. Chem., Int. Ed.*, 2018, **57**, 9859.
22 Y. Fang, L. Xiao, Z. Chen, X. Ai, Y. Cao and H. Yang, *Electrochem. Energ. Rev.*, 2018, **1**, 294.
23 Y. Fang, Q. Liu, L. Xiao, Y. Rong, Y. Liu, Z. Chen, X. Ai, Y. Cao, H. Yang and J. Xie, *Chem*, 2018, **4**, 1167.
24 J. Zheng, Y. Zhao, X. Feng, W. Chen and Y. Zhao, *J. Mater. Chem. A*, 2018, **6**, 6559.
25 J. Zhao, L. Zhao, K. Chihara, S. Okada, J.-i. Yamaki, S. Matsumoto, S. Kuze and K. Nakane, *J. Power Sources*, 2013, **244**, 752.
26 A. Ponrouch, E. Marchante, M. Courty, J.-M. Tarascon and M. R. Palacín, *Energy Environ. Sci.*, 2012, **5**, 8572.
27 X. Xia, M. N. Obrovac and J. R. Dahn, *Electrochem. Solid-State Lett.*, 2011, **14**, A130.
28 S. Komaba, W. Murata, T. Ishikawa, N. Yabuuchi, T. Ozeki, T. Nakayama, A. Ogata, K. Gotoh and K. Fujiwara, *Adv. Funct. Mater.*, 2011, **21**, 3859.
29 D. A. Stevens and J. R. Dahn, *J. Electrochem. Soc.*, 2001, **148**, A803.
30 X. Xia and J. R. Dahn, *J. Electrochem. Soc.*, 2012, **159**, A515.
31 N. Yabuuchi, K. Kubota, M. Dahbi and S. Komaba, *Chem. Rev.*, 2014, **114**, 11636.
32 G. J. Jung, Y. Lee, Y. S. Mun, H. Kim, J. Hur, T. Y. Kim, K. S. Suh, J. H. Kim, D. Lee, W. Choi and I. T. Kim, *J. Power Sources*, 2017, **340**, 393.
33 Y. Kim, K.-H. Ha, S. M. Oh and K. T. Lee, *Chem.–Eur. J.*, 2014, **20**, 11980.
34 L. Wu, H. Lu, L. Xiao, X. Ai, H. Yang and Y. Cao, *J. Mater. Chem. A*, 2015, **3**, 5708.
35 J. Zhao, L. Zhao, N. Dimov, S. Okada and T. Nishida, *J. Electrochem. Soc.*, 2013, **160**, A3077.
36 J. Zhao, J. Xu, D. H. Lee, N. Dimov, Y. S. Meng and S. Okada, *J. Power Sources*, 2014, **264**, 235.
37 X. Xia and J. R. Dahn, *Electrochem. Solid-State Lett.*, 2012, **15**, A1.
38 X. Xia and J. R. Dahn, *J. Electrochem. Soc.*, 2012, **159**, A1048.
39 X. Xia and J. R. Dahn, *J. Electrochem. Soc.*, 2012, **159**, A647.
40 K. Xu, *Chem. Rev.*, 2004, **104**, 4303.
41 R. Marom, O. Haik, D. Aurbach and I. C. Halalay, *J. Electrochem. Soc.*, 2010, **157**, A972.
42 I. A. Profatilova, N.-S. Choi, S. W. Roh and S. S. Kim, *J. Power Sources*, 2009, **192**, 636.
43 I. A. Profatilova, C. Stock, A. Schmitz, S. Passerini and M. Winter, *J. Power Sources*, 2013, **222**, 140.
44 I. A. Profatilova, S.-S. Kim and N.-S. Choi, *Electrochim. Acta*, 2009, **54**, 4445.
45 T. Kawamura, S. Okada and J.-i. Yamaki, *J. Power Sources*, 2006, **156**, 547.
46 Q. Wang, J. Sun and C. Chen, *J. Hazard. Mater.*, 2009, **167**, 1209.
47 Y.-S. Park and S.-M. Lee, *Bull. Korean Chem. Soc.*, 2011, **32**, 145.
48 L. Zhao, M. Zhou, T. Doi, S. Okada and J.-i. Yamaki, *Electrochim. Acta*, 2009, **55**, 125.
49 B. Zhang, G. Rousse, D. Foix, R. Dugas, D. A. Corte and J.-M. Tarascon, *Adv. Mater.*, 2016, **28**, 9824.
50 J. S. Gnanaraj, E. Zinigrad, L. Asraf, H. E. Gottlieb, M. Sprecher, M. Schmidt, W. Geissler and D. Aurbach, *J. Electrochem. Soc.*, 2003, **150**, A1533.
51 Q.-S. Wang, J.-H. Sun, G.-Q. Chu, X.-L. Yao and C.-H. Chen, *J. Therm. Anal. Calorim.*, 2007, **89**, 245.
52 T. Kawamura, A. Kimura, M. Egashira, S. Okada and J.-I. Yamaki, *J. Power Sources*, 2002, **104**, 260.
53 D. D. MacNeil and J. R. Dahn, *J. Electrochem. Soc.*, 2003, **150**, A21.
54 M. Metzger, B. Strehle, S. Solchenbach and H. A. Gasteiger, *J. Electrochem. Soc.*, 2016, **163**, A1219.